Neurochemistry International 56 (2010) 789–798

Contents lists available at ScienceDirect

Neurochemistry International

journal homepage: www.elsevier.com/locate/neuint

The norepinephrine transporter (NET) radioligand (S,S)-[^{18}F]FMeNER-D$_2$ shows significant decreases in NET density in the human brain in Alzheimer's disease: A post-mortem autoradiographic study

Balázs Gulyás [a,*], Damian Brockschnieder [b], Sangram Nag [a], Elena Pavlova [a], Péter Kása [c], Zsuzsa Beliczai [d], Ádám Légrádi [d], Károly Gulya [d], Andrea Thiele [b], Thomas Dyrks [b], Christer Halldin [a]

[a] Karolinska Institutet, Department of Clinical Neuroscience, Psychiatry Section, S-171 76 Stockholm, Sweden
[b] Bayer Schering Pharma AG, D-13353 Berlin, Germany
[c] University of Szeged, Department of Psychiatry, H-6720 Szeged, Hungary
[d] Department of Cell Biology and Molecular Medicine, Faculty of Medicine and Faculty of Sciences and Informatics, University of Szeged, H-6720 Szeged, Somogyi u. 4, Hungary

ARTICLE INFO

Article history:
Received 20 February 2010
Accepted 1 March 2010
Available online 6 March 2010

Keywords:
Norepinephrine transporter (NET)
(S,S)-[^{18}F]FMeNER-D2
Human brain
Alzheimer's disease (AD)
Whole hemisphere autoradiography
Receptor binding
Immunohistochemistry
LC
Thalamus
Positron emission tomography (PET)

ABSTRACT

Earlier post-mortem histological and autoradiographic studies have indicated a reduction of cell numbers in the locus coeruleus (LC) and a corresponding decrease in norepinephrine transporter (NET) in brains obtained from Alzheimer's disease (AD) patients as compared to age-matched healthy controls. In order to test the hypothesis that the regional decrease of NET is a disease specific biomarker in AD and as such, it can be used in PET imaging studies for diagnostic considerations, regional differences in the density of NET in various anatomical structures were measured in whole hemisphere human brain slices obtained from AD patients and age-matched control subjects in a series of autoradiographic experiments using the novel selective PET radioligand for NET (S,S)-[^{18}F]FMeNER-D$_2$. (S,S)-[^{18}F]FMeNER-D$_2$ appears to be a useful imaging biomarker for quantifying the density of NET in various brain structures, including the LC and the thalamus wherein the highest densities are found in physiological conditions. In AD significant decreases of NET densities can be demonstrated with the radioligand in both structures as compared to age-matched controls. The decreases in AD correlate with the progress of the disease as indicated by Braak grades. As the size of the LC is below the spatial resolution of the PET scanners, but the size of the thalamus can be detected with appropriate spatial accuracy in advanced scanners, the present findings confirm our earlier observations with PET that the *in vivo* imaging of NET with (S,S)-[^{18}F]FMeNER-D$_2$ in the thalamus is viable. Nevertheless, further studies are warranted to assess the usefulness of such an imaging approach for the early detection of changes in thalamic NET densities as a disease-specific biomarker and the possible use of (S,S)-[^{18}F]FMeNER-D$_2$ as a molecular imaging biomarker in AD.

1. Introduction

One of the major monamine neurotransmitters is norepinephrine (NE) or, with other term, noradrenalin. The major source of NE in the brain is the LC which is located in the rostral pons. Noradrenergic terminals in the brain are widespread and LC neurons project to the cerebral cortex, thalamus, cerebellum and neurons in brain stem nuclei (Smith et al., 2006). The NE system plays a role in various CNS functions including brain maturation, autonomic regulation processes, stress related actions, attention and memory functions. The system has been identified as a major biological underpinning of certain personality traits, as well. The dys-regulation and pathology of the NE system has been identified in several CNS pathologies, including neurodegenerative diseases, ADHD, schizophrenia and depression.

The norepinephrine transporter (NET), similarly to other transporter in the pre-synaptic cell membrane, plays a major role in the regulation of NE related actions at cellular levels (Schroeter et al., 2000; Sanders et al., 2005). As NET is responsible for the re-uptake of NE and, by this way, for the intra-synaptic NE levels, it is the target of several therapeutic drug actions as well as that of abused drugs. Furthermore, the concentration of the released NE in the extrasynaptic space (Vizi, 2000) is also regulated by NET.

The quest for identifying appropriate early disease biomarkers in Alzheimer's disease (AD) has been in the forefront of biomarker research in recent years. Amyloid and insoluble Aβ peptides have been identified as disease biomarkers (Andreasen and Zetterberg, 2008; Hampel et al., 2008; Svedberg et al., 2009) for which molecular imaging biomarkers have also been developed (Klunk et al., 2004; Nordberg, 2007, 2008; Cai et al., 2007). Activated

* Corresponding author.
E-mail address: balazs.gulyas@ki.se (B. Gulyás).

0197-0186/$ – see front matter © 2010 Elsevier Ltd. All rights reserved.
doi:10.1016/j.neuint.2010.03.001

microglia and the up-regulated peripheral benzodiazepine system (PBR/TSPO) (Banati, 2002; Venneti et al., 2006; Chen and Guilarte, 2008; Gavish et al., 1999) are other evident candidates, as are activated astrocytes and the MAO-B system (Schwab and McGeer, 2008; Fuller et al., 2009; Rodríguez et al., 2009; Razifar et al., 2006; Johansson et al., 2007). For these systems, molecular imaging biomarkers are already available (Kumlien et al., 1995; Reutens, 2000; Kassiou et al., 2005; Dollé et al., 2009; Gulyás et al., 2009; Fowler et al., 1995). Recently other target systems are also considered, including the NE system.

In AD a profound reduction of LC cell numbers by averaged 50–70% (compared to age-matched healthy controls) and a corresponding decrease in NET have consistently been documented by numerous post-mortem studies (Tejani-Butt et al., 1993; Lyness et al., 2003; Zarow et al., 2003). For this reason, the degeneration of LC in AD may bear important implications for both the early diagnosis and the treatment of the disease (Haglund et al., 2006) as it may serve as a disease biomarker for which molecular imaging biomarkers, as diagnostic agents, can be developed. Until today, only sporadic data have been available on the degeneration of the terminal fields of LC neurons (e.g. in the thalamus, the amygdala and the cortex) or about the existence of compensatory mechanisms, e.g. up-regulation of NET, in the LC and the aforementioned target regions (e.g. Hoogendijk et al., 1999; Szot et al., 2006). On the other hand, the degeneration of the LC has been correlated with the potentiation of amyloid-induced cortical inflammation in AD (Heneka et al., 2002, 2006; Kalinin et al., 2007) as well as behavioural changes (aggressive behaviour, cognitive impairment) in dementias (Matthews et al., 2002).

Consequently, early changes in brain NE and NET levels can serve as disease biomarkers in AD and other neurodegenerative diseases. NET-rich regions in the human brain may therefore serve as a target for diagnostic imaging, with special regard to early diagnosis of AD using molecular imaging techniques, including positron emission tomography (PET). Naturally, this would also require adequate molecular imaging biomarkers.

For long there have been two major obstacles in the way of a routine PET diagnostic approach using the imaging of NET in the human brain for early AD diagnosis: (i) the size of the LC in the human brain is below the spatial resolution of the currently used diagnostic PET scanners (usually between 3 and 6 mm) (German et al., 1988), and (ii) the lack of optimal diagnostic PET ligands for imaging the NET system.

Further to initial studies with carbon-11 labelled MeNER analogues (Wilson et al., 2003), with the introduction of the selective NET ligand (S,S)-[^{18}F]FMeNER-D$_2$ (Schou et al., 2004, 2005) an appropriate PET ligand has become available for the imaging community. Early PET studies on non-human primates and on humans have indeed demonstrated the usefulness of the novel ligand in the *in vivo* exploration of the NET system (Schou et al., 2004; Arakawa et al., 2008; Takano et al., 2008a,b,c; Takano et al., 2009a,b), as did studies with the tritiated analogue in in vitro experiments (Ghose et al., 2005). However, these early PET studies have also called our attention to the second aforementioned issue, namely that the size of the LC, is not an appropriate anatomical target for routine imaging studies of the NET system in humans. Alternatively, other anatomical structures with relatively high NET densities and volumes appropriate for diagnostic PET scanners may serve as perspective target structures for routine imaging procedures on early AD diagnosis in the future.

The main objective of the present investigation was threefold: (i) To explore the possible changes in NET densities in AD brains in comparison with age-matched control brains with the help of the prospective NET radioligand (S,S)-[^{18}F]FMeNER-D$_2$. (ii) To clarify whether there is a demonstrable reduction in NET in the thalamus, the prime projection structure of LC, whether this reduction goes parallel with that in the LC, and, consequently, the thalamus could also serve as a target region for PET imaging of NET in AD patients. (iii) To assess the possible use of (S,S)-[^{18}F]FMeNER-D$_2$ as a molecular imaging biomarker in AD in the future.

2. Experimental procedures

2.1. Radiochemistry

(S,S)-[^{18}F]FMeNER-D$_2$ (Fig. 1A), a radiolabelled analogue of reboxetine (2-(2-ethoxyphenoxy)-phenyl-methyl)morpholine (Fig. 1B), was prepared as described in detail elsewhere (Schou et al., 2004). Radiochemical purity was higher than 99%. The specific radioactivity was higher than 176 GBq/μmol.

2.2. Brain tissue

2.2.1. Whole hemisphere brain slices

Whole hemisphere brain sections from 10 AD cases, covering various Braak stages, and 10 age-matched, healthy controls have been investigated.

Human brains without pathology were obtained from the National Institute of Forensic Medicine, Karolinska Institute, Stockholm (n = 10). Ethical permission was obtained from the relevant Research Ethics Committee (Dnr. 01-161). The brains had been removed during forensic autopsy, were "freshly frozen" and were handled in a manner similar to that described previously (Hall et al., 1998; Varnäs et al., 2004). The deceased persons' age varied between 32 and 75 y, the causes of death were suicide, cardiovascular, and pulmonary embolism, the post-mortem time interval was between 2 and 23 h. The sectioning took place on a Leica cryomacrocut system. The resulting slices were horizontal slices of 100 μm thickness.

Ten brains from Alzheimer patients were obtained from the Alzheimer Research Group of the Albert Szent-Györgyi Medical and Health Science Center, University of Szeged. Ethical permission was obtained from the Research Ethics Committee of the University of Szeged (1895/2004). The post-mortem time interval was between 2.5 and 5.0 h. The patients' age was between 54 and 98 y, and the collection covered Braak stages between 0.5 and 5. The brains had been removed during clinical autopsy and were handled similarly to that described above. The sectioning took place on a Leica cryomacrocut system. The resulting slice thickness was 100 μm. Various coronal sections intersecting the parietal and temporal lobes, the basal ganglia and the hippocampus were used for the measurements.

The stipulation of the experiments was due to the autopsy and sectioning technique: The ten control brains were harvested in a dedicated manner for a post-mortem human brain bank and, consequently, they were sectioned horizontally and the LC is visible on the sections. The AD brains were obtained from clinical autopsies and coronal sections were made. The brainstem was not a part of the original slabs, and there is no LC on the coronal sections.

2.2.2. Brain blocks

Brain blocks (approximately 1 cm^3 in volume each) from 5 Alzheimer patients and 5 age-matched controls were obtained from the Netherlands Brain Bank (protocol number: 2007/526). In each case, from one hemisphere fresh frozen brain blocks were obtained from the following anatomical regions: brainstem containing the LC, thalamus, hippocampus, parietal and temporal lobes. From each block, slices of 20 μm thickness were cut and used for the autoradiography (ARG) studies. From the same brains' other hemisphere formaldehyde fixed (4%) and paraffin-embedded brain blocks were obtained from identical anatomical regions and 6 μm thick slices sections were used for immunohistochemical studies.

2.3. In vitro autoradiography

2.3.1. Whole hemisphere brain slices

Experimental procedures followed those described in Schou et al. (2005), with the exception of incubation time, which was shortened due to the use of a high sensitivity phosphorimager. The whole hemisphere sections were incubated for

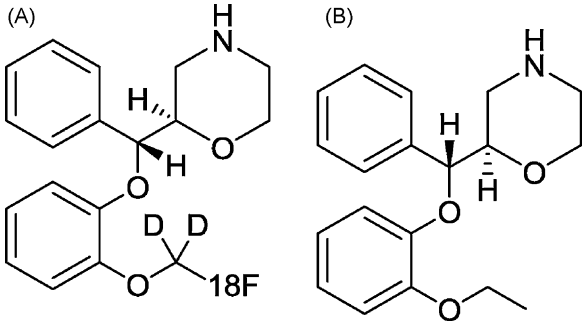

Fig. 1. Structure of (S,S)-[^{18}F]FMeNER-D$_2$ (A) and reboxetine (B).

55 min at room temperature (RT) with 0.02 MBq/mL (S,S)-[^{18}F]FMeNER-D$_2$ in a Tris buffer (50 mM, pH 7.4) containing sodium chloride (300 mM), potassium chloride (5 mM), and ascorbic acid (0.1%, w/v). The sections were then washed 3 × 5 min in the same buffer (at RT), then briefly dipped in ice cold distilled water. The readings were made in a Fujifilm BAS-5000 phosphorimager and digitized using a Fujifilm IP Eraser 3. Standards were prepared by serial dilution of the radioligand stock solution in assay buffer. Aliquots (2 μL) of the standards were spotted onto polyethylene-backed absorbent paper (BenchGuard), allowed to dry, scanned and digitized in the phosphorimager parallel with the tissue scans. From the known specific activity of the radioligand, the corresponding concentration (fmol) of radioligand was calculated and the correlation between the amount of the standard (kBq) and the phosphorimager signal was established. The specific binding values were calculated by using the total binding values and the non-specific binding values, determined in the excess of nisoxetine (10 μM).

2.3.2. Binding assay on slices from small brain blocks

Before application of the autoradiographic technique to the AD tissue, using brain blocks (hippocampus) from the control material we identified optimal conditions for labeling of NET with (S,S)-[^{18}F]FMeNER-D$_2$ for various parameters, including optimal ligand concentration, temperature and incubation time, in a series of saturation experiments with increasing ligand concentrations, incubation times and temperatures.

LC consecutive tissue sections (20 μm) in triplicates were used. In order to determine the K_D value and the optimal ligand concentration, first saturation of (S,S)-[^{18}F]FMeNER-D$_2$ binding was performed at 22 °C (RT) and at 37 °C. Tissues were incubated with (S,S)-[^{18}F]FMeNER-D$_2$ at five concentrations in the range between 0.02 and 120 nM in Tris buffer (pH 7.4) for 90 min. Parallel incubations were carried out with consecutive sections in the same incubation medium with 10 μM nisoxetine added. The sections were then washed twice with the same buffer and finally dipped into distilled water once. After drying, sections were exposed to the phosphor imaging plate for 3 h. The Fujifilm IP Eraser 3 was used to erase the images from the plates in the image-reading unit of the Phosphor Imager (Fujifilm BAS-5000). Optical densities were digitized and analyzed using an image analysis program MultiGauge V3.0.

For quantification, individual calibration standards were prepared for each set of the brain sections exposed to the same imaging plate. The standards were 20 μL drops of (S,S)-[^{18}F]FMeNER-D$_2$ from the incubation solution (solutions with 3 different concentrations [0.0001, 0.004 and 60 MBq/mL] were used) placed on a thin, absorbent paper and exposed simultaneously with the brain sections. Knowing the concentration and the volume of the standard sample (the drop with the optical density closest to the section's optical densities was chosen for calculations), the amount of substance expressed in fmol was calculated (Johnström and Davenport, 2005). The total counts over the standard, measured by the phosphor imaging system, allowed the calculation of calibration factor in counts per fmol. Using the GraphPad Prism software and knowing number of counts per square millimeter for each ROI and calibration factor, we converted it to fmol per square millimeter and then to fmol per cubic millimeter. Similarly, curves obtained with GraphPad Prism were used to determine K_D and B_{max} values.

In order to optimise incubation times, the brain slices were incubated with (S,S)-[^{18}F]FMeNER-D$_2$ at the concentration of 0.4 MBq/mL (which corresponded to 3.68 nM) for different incubation times (2, 5, 20, 60, 120 and 180 min) at RT as well as at 37 °C. Parallel incubations were carried out with 10 μM nisoxetine added. In another series, this optimal ligand concentration was replaced by a sub-optimal ligand concentration corresponding to 0.04 MBq/mL, in order to test concentration dependence of the signal in the key structures. Equilibrium was achieved at both temperature conditions, although faster at the 37 °C (after approximately 45 min) than at RT (after approximately 120 min).

In the first binding assay series, using optimised experimental conditions, LC and thalamus from 5 controls and 5 AD brains were investigated. Tissues were incubated with (S,S)-[^{18}F]FMeNER-D$_2$ at the concentration of 0.4 MBq/mL (3.68 nM) for 120 min at RT. 10 μM nisoxetine was used as a blocker in the parallel sections. Specific binding was obtained after subtraction of non-specific binding from total binding.

2.4. Histochemistry and immunohistochemistry

Paraffin-embedded tissue sections were deparaffinated, hydrated and stained in a 0.1% toluidine blue solution containing 0.1% boric acic for 1 min. After rinsing in distilled water for a few seconds, the sections were dehydrated quickly through 95% and two-changes of 100% ethanol, cleared in xylene for 2 × 3 min, and coverslipped in DPX mounting medium. For the demonstration of the presence of tau proteins in affected neurons as well as amyloid plaques and reactive astrocytes in the same brains from which the fresh frozen brain slices for autoradiographic experiments were prepared, we used (1) AT8 monoclonal antibodies with diaminobenzidine (DAB) enhancer for tau protein recognition, (2) GFAP monoclonal antibody or (3) a combination of tau or GFAP signal (with fluorescence enhancement) and thioflavine S amyloid plaque labeling Kelényi (1967) on paraffin-embedded brain sections (Amsterdam material). Immunohistochemistry was performed according to Kortvely et al. (2003).

2.4.1. Tissue preparation for immunohistochemistry

The paraffin-embedded sections were fixed in 0.1 M TBS (Tris-buffered saline; pH 7.5) containing 4% formaldehyde for 10 min and washed for 3× 5 min in 0.1 M TBS at room temperature (RT). The paraffin-embedded sections were incubated in 0.05 M Tris–HCl solution (pH 7.6) containing 0.1% trypsin and 0.1% $CaCl_2$ for 15 min in a humidified chamber at 37 °C. After blocking the endogenous peroxidase in 1% H_2O_2 for 15 min at RT, the sections were washed for 3× 5 min in 0.1 M TBS at RT. The tissue sections were permeabilized and the background binding of the antibodies was reduced in a blocking solution (0.1 M TBS solution containing 5% NGS (normal goat serum), 1% BSA (bovine serum albumin), 0.05% Triton X-100) for 30 min at 37 °C. Sections were covered with a solution containing mouse anti-tau primary antibody (AT-8; Pierce) diluted to 1:1000 in the blocking solution at 4 °C overnight, then washed for 4× 10 min in 0.1 TBS at RT.

2.4.2. DAB immunohistochemistry

The sections were treated with an anti-mouse IgG secondary antibody diluted (1:200) in a blocking solution (where Triton X-100 was omitted) for 5 h at RT. After several washes (4× 10 min), biotinylated streptavidin-peroxidase tertiary antibody (1:200) in a blocking solution (without Triton X-100) was applied to the sections overnight at 4 °C. The sections were washed again in 0.1 M TBS for 4× 10 min at RT and processed for peroxidase enzyme histochemistry. The sections were pre-incubated in filtered 0.1 M TBS solution containing 0.5 mg/mL 3,3′-diaminobenzidine (DAB) for 20 min at RT, and then developed in the same solution but also containing 0.01% H_2O_2 for 20 min at RT. The sections were washed for 3× 5 min in 0.1 M TBS and then dipped into distilled water for a few seconds. The cell nuclei were stained in 0.1% toluidine solution for 1 min, washed in distilled water for 1 min, dehydrated in a series of ethanol solutions, covered with DPX (distrene plasticizer xylene) and cover-slipped.

2.4.3. Tau and GFAP immunohistochemistry (Alexa)/amyloid staining with Thioflavin S

The sections were treated with Alexa 568-conjugated anti-mouse IgG secondary antibody diluted (1:1000, Invitrogen^{TM}) in a blocking solution (where Triton X-100 was omitted) for 5 h at RT. After several washes (4× 10 min) in 0.1 M TBS the cell nuclei were stained in 0.1 M TBS containing 1 mg/mL polyvinylpyrrolidine and 0.5 μL/mL Hoechst 33258 dye (Hoechst). The sections were then rinsed for 2× 5 min in 0.1 M TBS containing 1 mg/mL polyvinylpyrrolidine solution and processed for amyloid plaque staining. The sections were stained with Mayer hematoxylin solution (100 mg hematoxylin, 20 mg Na-iodate, 5 g aluminum potassium sulfate, 5 g trichloroacetaldehyde nitrate, 100 mg citric acid) for 5 min at RT. After washing the sections in filtered tap water for 5 min, they were stained in 1 mg/100 mL thioflavin S solution. The sections were finally washed for 5 min in distilled water, air-dried overnight, covered with Vectashield and cover-slipped.

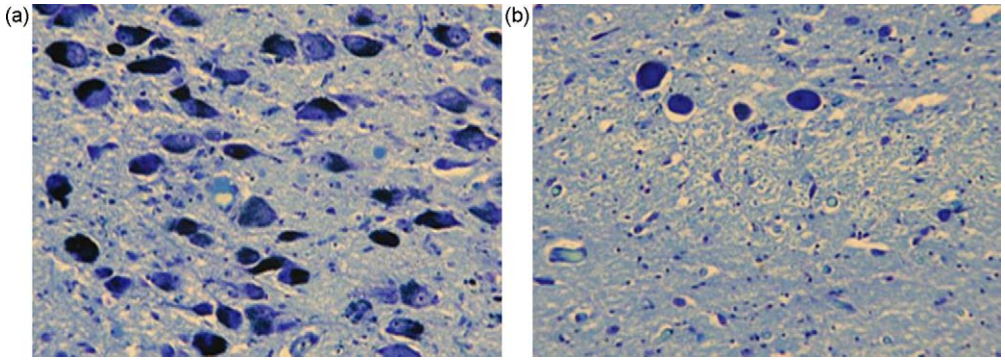

Fig. 2. Toluidine blue staining of NET containing neurons in the LC of control (A) and AD (B) brains. (Magnification made with a 5× objective; sections made across the longitudinal axis of the LC in both cases. Origin of tissue: Netherlands Brain Bank.)

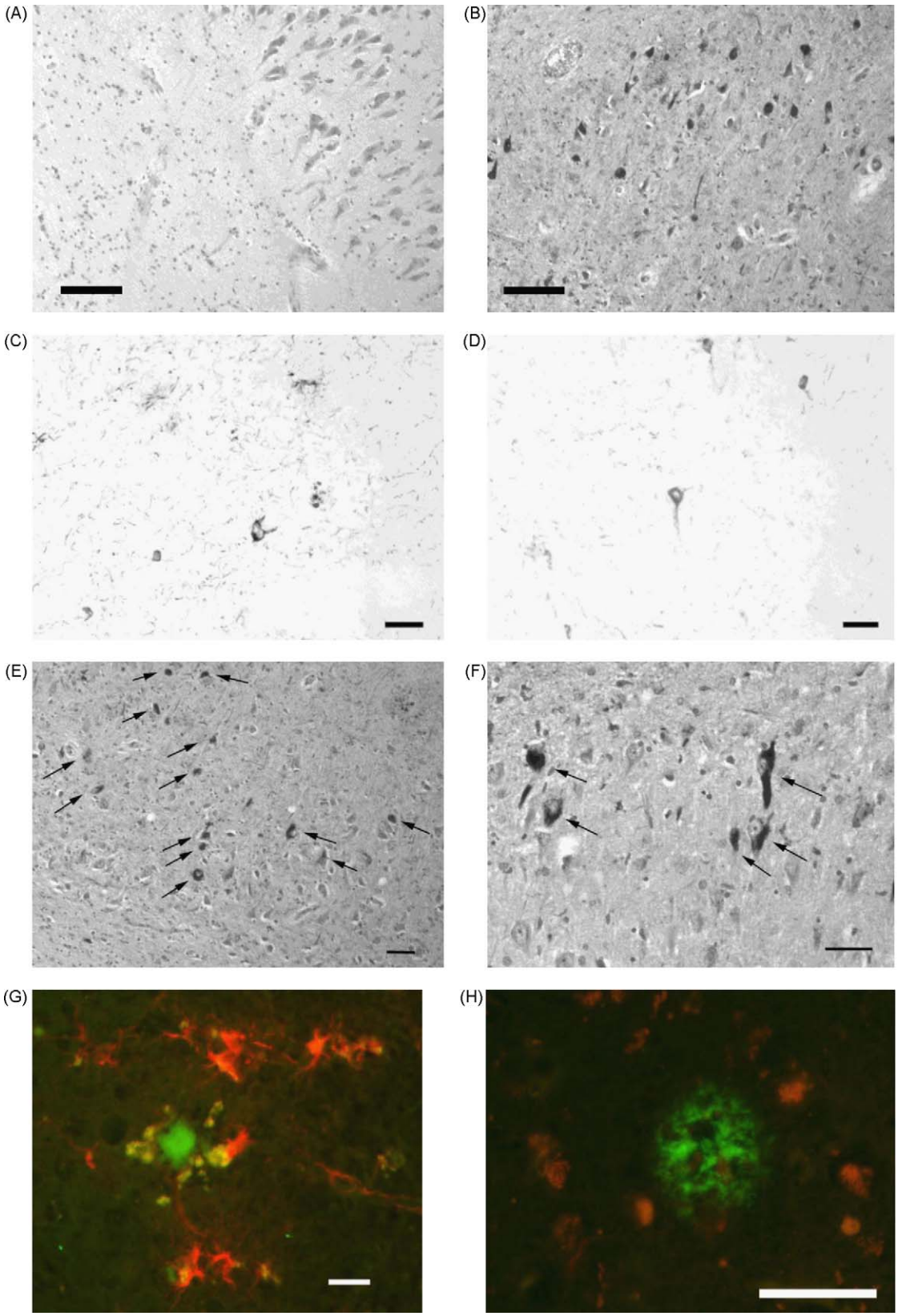

Fig. 3. Tau and GFAP immunoreactivity around the amyloid plaques in the hippocampi of paraffin-embedded sections of control and AD brains (A, B). The non-demented, control brain (Amsterdam material 00-142) was staged as Braak 1, while the Alzheimer's diseased brain (02-080) was diagnosed as Braak 5. The hippocampus in the control brain did not show tau immunopositivity (A), while the hippocampus from the AD sample displayed a large number of tau positive neurons (B). Scale bars for A and B: 200 μm. Detection of tau (C–F and H) and GFAP (G) immunoreactivities around the amyloid plaques in the gyrus temporalis and the hippocampus of AD brains. The samples were from the Amsterdam material: 05-071, gyrus temporalis, Braak 6 (C, D, F); 02-080, hippocampus, Braak 5 (E); 05-012, gyrus temporalis, Braak 6 (G). Tau positive neurons (arrows) in the gyrus temporalis (C, D, F) and the hippocampus (E) were detected by DAB staining (see Materials and Methods). A number of GFAP positive astrocytes (G) and tau positive neurons (H) (red immunofluorescence) could be seen around the amyloid plaques stained with thioflavin S (green fluorescence) in the hippocampus. Scale bars for C–H: 100 μm.

3. Results

3.1. Histology. Demonstration of cell loss in the LC

Cell densities in the LC were demonstrated using toluidine blue stain. The stain indicated a significant loss of LC neurons in the AD sections as compared to the sections obtained from age-matched control brains (Fig. 2).

3.2. Immunohistochemical verification of presence of Alzheimer pathology in AD samples

Immunohistochemical studies of AD brains, in contrast to age-matched control brains, indicated a clear-cut signal for both the anti-tau/DAB stain and the double staining with tau antibody (Alexa 568 detection) and thioflavine S stain, confirming the presence of amyloid beta and tau pathology. GFAP positive reactive astrocytes were also present around the amyloid plaques. In the control brains there was no positive signal for either stain (data not shown). In the AD brains both stains showed positive signals in various brain structures (Fig. 3).

3.3. Autoradiography in whole hemisphere brain sections: regional binding parameters

Visual examples from control brains are shown in Fig. 4. As shown on the whole hemisphere horizontal slices at the levels of the LC (*panels A, B, E, F*) and the thalamus (*panels C, D, G, H*), there is a high uptake of (S,S)-[^{18}F]FMeNER-D$_2$ in the LC which can be clearly blocked by an excess of nisoxetine. Also, there is a clear uptake in the thalamus, which is significantly reduced by an excess of nisoxetine. As shown in the images, the uptake of the radioligand was not homogeneous in the cortex and the various sub-cortical structures. The comparison between control and AD brains indicated relatively higher ligand uptake in cortical structures in AD brains, in line with earlier publications on eventual compensatory increases in NET densities in the projection regions of LC in AD (Fig. 5).

The quantitative analysis of the samples indicated that in control brains the highest mean specific binding was in the LC (34.8 fmol/mm^3), followed by approximately ten times lower binding in the thalamus (4.2 fmol/mm^3). This was followed by the lateral geniculate nucleus (LGN; 3.8 fmol/mm^3), the frontal lobe and putamen (3.6 fmol/mm^3), the occipital, temporal and parietal lobes (3.3, 2.5 and 0.6 fmol/mm^3), respectively, and other sub-cortical structures (Table 1).

In the AD brains the measuring of regional binding in all identical structures present in the horizontal slices (control material was not possible due to technical limitations coronal sectioning). Despite this technical limitation, the binding values in the comparable structures show in some cases marked differences between control and AD brains, but the effect's significance cannot be assessed due to the small sample size (Table 1).

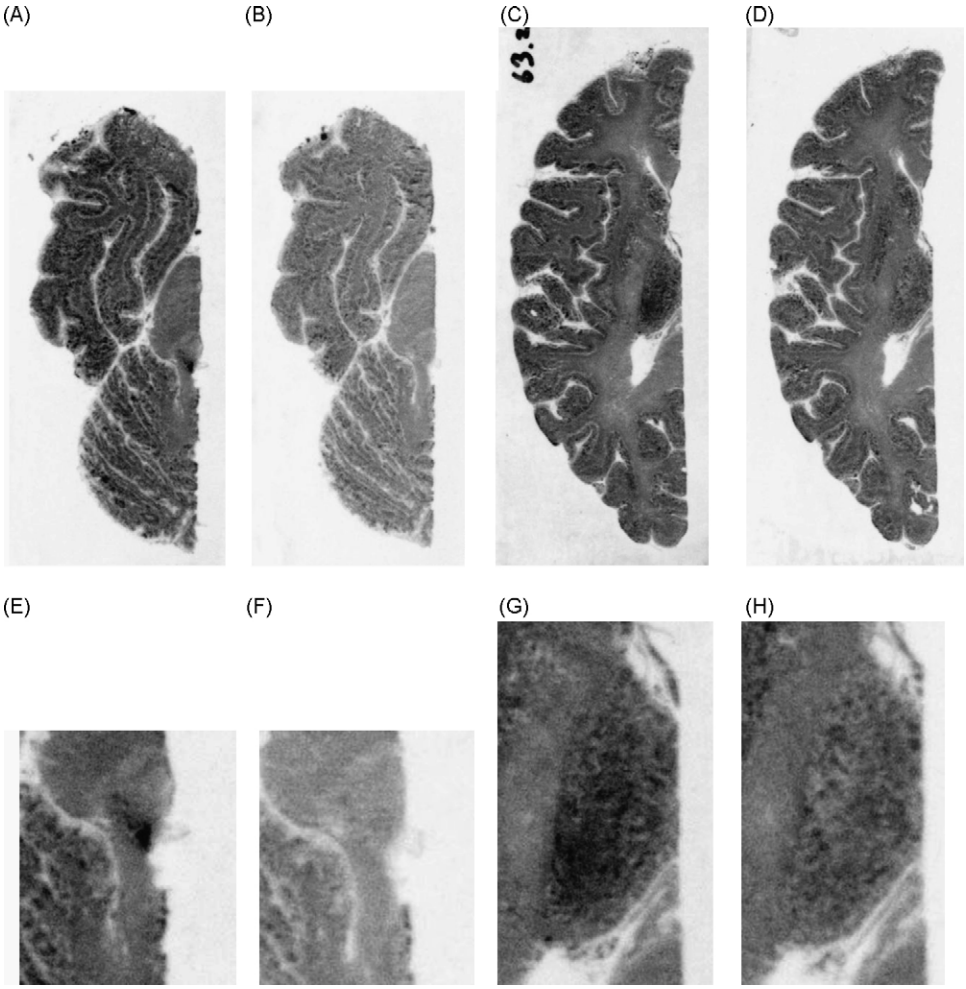

Fig. 4. Control brain (70 y male), horizontal slices, ARG with (S,S)-[^{18}F]FMeNER-D$_2$. A, C, E and G: baseline condition, B, D, F and H: blocking with 10 μM nisoxetine. A–D: whole hemisphere slices at the level of the LC (A and B) and the thalamus (C and D). E and F: LC magnified. G and H: Thalamus magnified.

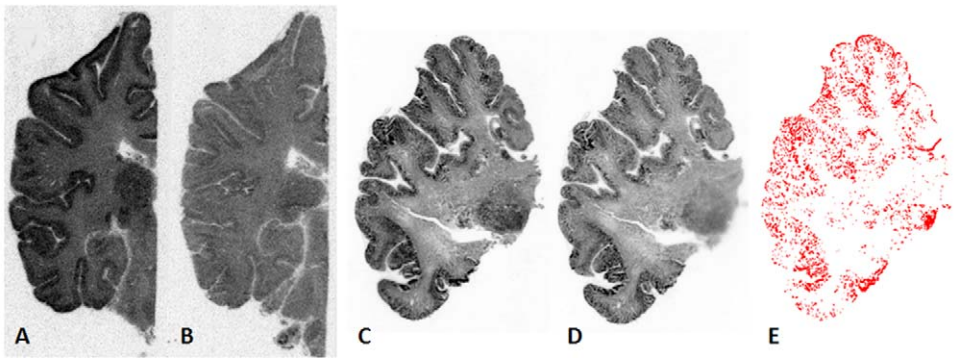

Fig. 5. Whole hemisphere autoradiography with (S,S)-[^{18}F]FMeNER-D$_2$ in baseline condition in an age matched control brain (horizontal slices, 33 y male) (A: baseline [total binding], B: blocking with 10 μM nisoxetine [non-specific binding]) and an AD brain (coronal slices, 50 y old female, Braak 2/3) (C: baseline [total binding], D: blocking with 10 μM nisoxetine [non-specific binding], E: 'total binding – non-specific binding' subtraction image, showing specific binding).

Table 1
Mean specific binding values (B_{max}; in fmol/mm^3, blocking with nisoxetine) in various brain structures obtained from whole hemisphere AD and control brain sections (n = number of brains). The brain samples belong to those obtained by the Karolinska Institute (controls, total n = 10) and the University of Szeged (AD, total n = 10). Due to the differences in sampling and sectioning, the control brains (sectioned coronally) contain more structures than the AD brains (obtained from pathology obductions after routine macroscopic neurohistological examinations and sectioned horizontally; consequently, a number of structures are not present).

Brains	Control			AD		
Structures	B_{max}	SEM	n	B_{max}	SEM	n
LC	34.8	3.0	7	n.a.	–	–
Thalamus	4.2	1.5	8	1.7	1.9	3
LGN	3.8	–	1	n.a.	–	–
Frontal	3.6	1.0	9	0.5	–	1
Putamen	3.6	1.5	8	n.a.	–	–
Temporal	2.5	1.0	10	2.8	2.1	3
Parietal	0.6	2.1	2	4.0	1.3	2
Occipital	3.3	1.9	4	n.a.	–	–
Hippocampus	1.6	0.8	3	0.6	–	1
Cerebellum	1.0	0.5	8	n.a.	–	–
White matter	0.9	0.7	10	1.4	1.3	3

3.4. Autoradiography in small brain sections

Analysis of the quantitative assays using small brain block slices in triplicates at RT resulted in the following values for the binding parameters: K_D = 3.6 nM and B_{max} = 84.3 fmol/mm^3.

Using both radioactivity concentrations (0.4 and 0.04 mBq/mL), there was a marked difference in specific binding between AD and control brains in the LC and thalamus whereas there appeared to be no marked difference in other structures (hippocampus, temporal, parietal lobes). In the thalamus this marked difference at 0.04 MBq/mL did not reach significance (p = 0.1711), at 0.4 MBq/mL radioactivity concentrations the difference between AD and age-matched control brains was significant (p = 0.0353) (Fig. 6).

3.5. Correlation between Braak grades and binding

Using 0.4 MBq/mL radioactivity concentration in the autoradiographic experiments, we found a significant negative correlation between Braak grades and specific binding in both the LC and the thalamus in the 20 μm thick brain slices obtained from the small brain blocks including control (Braak 0–1) and AD (Braak 2–6) material ("Amsterdam brains") (Fig. 7). Due to the low r^2 value, however, this significant correlation should be considered as a preliminary observation which warrants further experiments to assess the robustness of the correlation.

4. Discussion

Norepinephrine (NE) is one of the major monoamine neurotransmitters in the primate brain. Noradrenergic neurons in the human brain are predominantly located in the LC, but other regions, including the lateral tegmental areas, also contain cells producing norepinephrine. The axons of these noradrenergic neurons reach target neurons in various brain regions, including the thalamus, the amygdala, the cingulate cortex, hypothalamus and hippocampus, and the striatum, as well as cells in the spinal cord.

The norepinephrine transporter (NET), a membrane glycoprotein with 12 membrane-spanning domains, is the protein regulating the re-uptake of NE from the synapse. NET is an important target site for several CNS drugs, including antidepressants, as well as drugs of abuse. Using autoradiographic techniques with labelled NET ligands, such as [^{3}H]nisoxetine, it has been demonstrated that NET concentrations in the rodent brain are highest in the LC, followed by the dorsal raphe nuclei (Ordway et al., 1997). Other brain regions, rich in NET, are those which have been identified as the main target regions of NE neurons.

Changes in NET density may be result of genetic polymorphism, neurological and psychiatric diseases, physiological ageing or the pharmacological effects of therapeutic or abused drugs (Klimek et al., 1997; Tellioglu and Robertson, 2001). Due to its early decrease in neurodegenerative diseases, including AD, NET appears to be a useful biomarker of disease. The present investigation focused predominantly on this issue, namely, what the quantitative change of NET density is in the various brain structures in AD and to what extent these changes correlate with disease progression. Furthermore, the question that which of the various structures in the human brain, rich in NET in healthy subjects but loosing NET in AD, can be used as prospective target regions in PET studies using (S,S)-[^{18}F]FMeNER-D$_2$ as an imaging biomarker, was also tackled, with special regard to the possible role of the

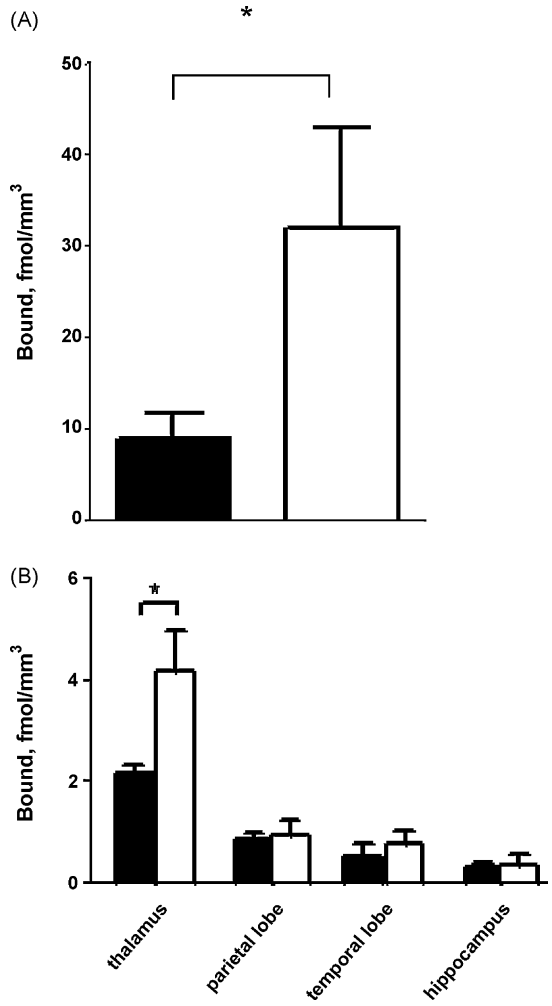

Fig. 6. (A) Specific binding (fmol/mm^3) in the LC in AD (black column) and age. Matched control (white column) brains. The difference in the LC between AD and control brains was significant. Results obtained with 0.4 MBq/mL ligand concentration and nisoxetine as the blocker. Errors bars indicate SEM, significant differences ($p < 0.05$) between average values are indicated by asterisk. (B) Specific binding (fmol/mm^3) in the thalamus, parietal and temporal lobes and the hippocampus in AD (black columns) and age-matched control (white columns) brains. Results obtained with 0.4 MBq/mL ligand concentration and nisoxetine as the blocker. Errors bars indicate SEM, significant differences ($p < 0.05$) between average values are indicated by asterisk. The difference in the thalamus between AD and control brains was significant ($p < 0.05$). Please note the scaling difference between the previous and present figures.

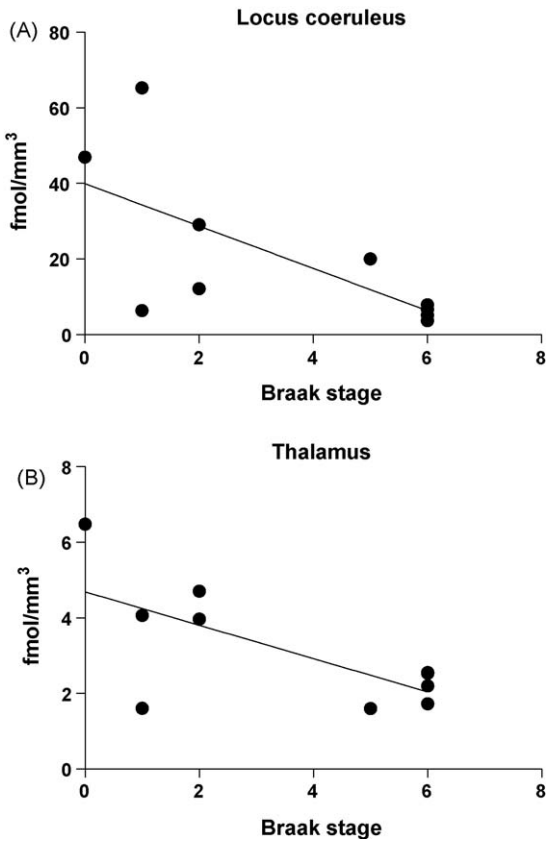

Fig. 7. Correlation between Braak grades and specific binding (fmol/mm^3) in the LC (A) and the thalamus (B). LC: slope: -5.607 ± 2.175, $r^2 = 0.4537$, $p = 0.0327$ (significant). Thalamus: slope: -0.4415 ± 0.1661, $r^2 = 0.4688$, $p = 0.0289$ (significant).

thalamus. On the other hand, due to its limited focus, the present investigation did not aim at exploring in detail various important corollaries of the decrease of NET in LC and other brain structures, including the compensatory NE increase due to the loss of NET.

4.1. Methodological considerations

In the present experiments we have used two autoradiographic approaches, each having respective advantages over the other, but also stipulations. The main advantage of whole hemisphere human autoradiography is that it displays receptor distributions in whole brain sections, thereby the regional distribution patterns can be studied both quantitatively and qualitatively. In addition to a unique technical background and expertise, this requires, however, huge amounts of radioligands and imaging plates, i.e. due to technical and financial stipulations the technique should be used "economically". Autoradiography assays in human brain slices, obtained from smaller blocks, require relatively less radioligand and can, therefore, be used more "economically" for quantification studies of ligand binding. But it has serious limitations, namely that only limited anatomical structures in the brain can be visualised. The brain slices used for the two techniques differ in thickness as for whole hemisphere autoradiography the slice thickness is usually around 100 μm, whereas it is only between 12 and 30 μm for small slice studies. This fact has consequences regarding the concentration of the radioligand as well as the quantification of the binding values.

Keeping in mind these considerations we resorted to small brain slice autoradiography for establishing optimised experimental conditions and determining some of the basic binding parameters of the ligand as well as to assess the concentration dependency of the binding. On the other hand, we used whole hemisphere autoradiography with a "one-point condition approach" to qualitatively and quantitatively explore the distribution and binding of the radioligand. The binding assay on the 20 μm thick small block brain slices established an optimal ligand concentration (0.4 MBq/mL), but it has also shown that lower, "sub-optimal" concentrations, such as 0.04 MBq/mL may also mirror the NET distribution in the brain faithfully. Keeping in mind this fact and the differences in ligand uptake between thin and thick slices (Varnäs, 2005), the 0.02 MBq/mL concentrations in the "one-point condition approach" should faithfully represent the transporter densities in various brain regions at the given concentration.

In the autoradiography literature binding data are usually normalised to mg tissue (as, for instance, in a former publication by our group: Gulyás et al., 2009) or to mg protein (as, for instance, in Tejani-Butt et al., 1993; Ordway et al., 1997; Klimek et al., 1997). In the present study, with an eye on avoiding compensation for

volume loss, we have chosen to normalise the binding data to volume tissue (fmol/mm^3) due to that fact that preliminary histological studies indicated a significant loss of cells in LC.

4.2. NET distribution in normal brains

The present findings support earlier observations by other studies, using autoradiographic measurements on post-mortem human brain tissue. Ordway et al. (1997), using [^{3}H]nisoxetine, demonstrated high NET densities in the LC and the dorsal raphe nuclei, the binding varying between 97.7 and 299.8 fmol/mg protein in the dorsal raphe, between 75 and 101 fmol/mg protein in the median raphe nuclei, and between 78 and 293 in the LC. In the LC and the raphe nuclei Klimek et al. (1997), also using [^{3}H]nisoxetine, have shown binding values in the range of 150–200 fmol/mg protein in control subjects, and markedly reduced values in depressive patients. In the case of the caudal LC the reduction in binding values was significant. These observations have been supported by human autoradiographic data using (S,S)-[^{18}F]FMeNER-D$_2$ (Schou et al., 2005). In the non-human primate brain, using [^{3}H]nisoxetine, Smith et al. (2006) found the highest binding values in the LC (219.63 fmol/mg wet weight tissue) followed by the sub-coeruleus nucleus and the raphe. *In vivo* PET measurements yielded further support to this regional distribution pattern, using (S,S)-[^{18}F]FMeNER-D$_2$ in both non-human primates (Schou et al., 2004; Seneca et al., 2006) and humans (Takano et al., 2008a,b,c).

In the present experiments we measured specific binding in the presence of an excess of nisoxetine and expressed it in fmol/mm^3 of tissue. NET density in the LC is approximately an order of magnitude higher (between 35 and 40 fmol/mm^3) than NET densities in the thalamus, the LGN, the basal ganglia, hippocampus and cortex (between 2 and 5 fmol/mm^3). Other brain structures, including the cerebellum, brainstem and white matter, display even lower NET densities.

With respect to *in vivo* imaging of the human brain, the gradual decrease of binding among the cortical and sub-cortical structures should not, however, mislead us regarding the usefulness of these structures in molecular imaging studies on the human brain. As the LC's volume is only 0.10–0.15 cm^3, the LC would not be a useful imaging target in functional neuroimaging studies. Furthermore, as we have shown that the cortical uptake of the ligand is cell layer specific, the cortex per se does not seem to be an appropriate imaging target either. The thalamus (volume: 8.1–9.1 cm^3), a prime projection structure of LC, however, may be a prospective candidate of a target region in PET studies (Tuohy et al., 2004; Andrews et al., 1997).

4.3. NET distribution in AD brains

Classical histochemical and immunohistochemical techniques showed a marked decrease in NET positive cells in the LC of AD brains as compared to control brains. Furthermore, they have justified the diagnosis by displaying post-mortem histological and morphological signs of AD in the diseased brains (Thal and Braak, 2005).

In line with earlier studies (Tejani-Butt et al., 1993; Szot et al., 2000, 2006; Haglund et al., 2006) there is a marked (though non-significant, $p = 0.0735$) decrease in NET densities in the LC in AD patients as compared to age-matched controls. This observation, however, needs a technical comment. The determination of the exact location of the LC in diseased brains was not possible, as due to the loss of neurons neither the classical histological techniques nor the autoradiographic investigation was able to outline the borders of the LC. The operational definition of the LC in these cases was based upon the macroanatomical landmarks, including the midline and the contours of the brain stem. Should one be able to find the appropriate borders of the LC in the advanced AD cases, one would expect to have a better significance value regarding the loss of NET densities in AD as compared to age-matched control material.

In the thalamus we found a significantly lower NET density in AD than in control brains ($p = 0.0353$), whereas no marked changes were observed in other brain structures between AD and control brains. In comparison with the finding in the LC, this fact may underline the importance of reliable anatomical boundaries, used for the determination of the region of interest. The relatively large thalamus (8–9 cm^3; see above) may indeed serve as a region of interest for both post-mortem and *in vivo* studies on the determination of NET densities in AD vs. control brains.

There was a significant negative correlation ($p < 0.05$) between the Braak grades of the AD brains and NET densities, as measured by specific binding values, in both the LC and the thalamus, indicating that the progress of disease entails a steady and gradual loss of NET neurons in these structures.

4.4. The potential of (S,S)-[^{18}F]FMeNER-D$_2$ as a PET imaging biomarker

Recent molecular imaging studies by our group have demonstrated the usefulness of (S,S)-[^{18}F]FMeNER-D$_2$ as a PET radioligand for NET in the non-human primate brain and the human brain (Takano et al., 2008a,b,c, 2009a,b). The investigations were performed in healthy animals and human subjects. The present investigations aimed at exploring the ligand's potential use in diseased human brains, with special regard to AD, as an early molecular imaging biomarkers.

In the present context, a number of considerations should be carefully explored and deliberated. A major issue is the volumes of the target structures in the brain. As mentioned, the primary target structure, the LC, is in the range of 0.1 cm^3. It can be visualised with a high resolution research scanner (HRRT), as shown by our group (Takano et al., 2008a,b,c). However, this approach can hardly be used in routine clinical diagnostic practice. The thalamus, having a significantly larger volume (approximately 9 cm^3), appears to be a more adequate target structure in routine PET investigations in this regard. In healthy human brain the NET density differences between the LC and thalamus are 10-fold and this appears to be sufficient for imaging studies in healthy volunteers with an appropriate research scanner as demonstrated by our former *in vivo* PET studies (Takano et al., 2008a,b,c). The conundrum is whether in AD patients, wherein both the volume of these target structures and the density of NET heavily decreases, the successful imaging of NET is still possible with the present radioligand and imaging approach.

A further consideration should concern the relationship between NET density in the human brain and the affinity of (S,S)-[^{18}F]FMeNER-D$_2$. According to the herewith presented data, the density of NET in the thalamus is about 4.2 nM (Table 1), while the affinity of (S,S)-[^{18}F]FMeNER-D$_2$ is around 3.6 nM, giving rise to a B_{max}/K_D ratio of 1.17. In diagnostic imaging practice, for successful imaging an in vitro B_{max}/K_D ratio of at least 3 or higher is usually sought. Despite this expectation (S,S)-[^{18}F]FMeNER-D$_2$ has proven to be the only acceptable PET ligand of NET until today (Takano et al., 2008a,b,c, 2009a,b). To satisfactorily answer the question whether the ligand may serve as a useful molecular imaging biomarker for early identification of AD and for monitoring disease progression, further studies are warranted.

5. Summary and conclusion

There are significant decreases in NET density in the LC and the thalamus in AD brains as compared to age-matched controls. In

both cases, the decreases negatively correlate with increasing Braak grades and, thus, can serve as a biomarker of disease. Whereas the LC is a small nucleus in the human brain, the human thalamus, the primary projection structure of LC, due to its volume and the hereby demonstrated significant decrease in NET densities in AD brains as compared to age-matched control brains, may serve as a target region in functional neuroimaging studies with PET for the detection of changes in NET densities in suspected AD patients. Finally, the present data warrant further investigations regarding the possible use of (S,S)-[^{18}F]FMeNER-D$_2$ as a molecular imaging biomarker in AD.

Acknowledgements

The authors express their gratitude to Siv Eriksson for the outstanding technical assistance in preparing the whole hemisphere brain slices and for participation in the autoradiography experiments, to Dr. Randy Blakely for antibodies, and to Dr. Inge Huitinga and the Netherlands Brain Bank for brain tissue. This study was in part funded by Bayer Schering Pharma AG, Berlin, and in part by the EC-FP6-project DiMI, LSHB-CT-2005-512146.

References

Andreasen, N., Zetterberg, H., 2008. Amyloid-related biomarkers for Alzheimer's disease. Curr. Med. Chem. 15, 766–771.

Andrews, T.J., Halpern, S.D., Purves, D., 1997. Correlated size variations in human visual cortex, lateral geniculate nucleus, and optic tract. J. Neurosci. 17, 2859–2868.

Arakawa, R., Okumura, M., Ito, H., Seki, C., Takahashi, H., Takano, H., Nakao, R., Suzuki, K., Okubo, Y., Halldin, C., Suhara, T., 2008. Quantitative analysis of norepinephrine transporter in the human brain using PET with (S,S)-^{18}F-FMeNER-D2. J. Nucl. Med. 49, 1270–1276.

Banati, R.B., 2002. Visualising microglial activation in vivo. Glia 40, 206–217.

Cai, L., Innis, R.B., Pike, V.W., 2007. Radioligand development for PET imaging of beta-amyloid (Abeta)—current status. Curr. Med. Chem. 14, 19–52.

Chen, M.K., Guilarte, T.R., 2008. Translocator protein 18 kDa (TSPO) molecular sensor of brain injury and repair. Pharmacol. Ther. 118, 1–17.

Dollé, F., Luus, C., Reynolds, A., Kassiou, M., 2009. Radiolabelled molecules for imaging the translocator protein (18 kDa) using positron emission tomography. Curr. Med. Chem. 16, 2899–2923.

Fowler, J.S., Wang, G.J., Logan, J., Xie, S., Volkow, N.D., MacGregor, R.R., Schlyer, D.J., Pappas, N., Alexoff, D.L., Patlak, C., Wolf, A.P., 1995. Selective reduction of radiotracer trapping by deuterium substitution: comparison of carbon-11-L-deprenyl and carbon-11-deprenyl-D$_2$ for MAO B mapping. J. Nucl. Med. 36, 1255–1262.

Fuller, S., Münch, G., Steele, M., 2009. Activated astrocytes: a therapeutic target in Alzheimer's disease? Expert Rev. Neurother. 9, 1585–1594.

Gavish, M., Bachman, I., Shoukrun, R., Katz, Y., Veenman, L., Weisinger, G., Weizman, A., 1999. Enigma of the peripheral benzodiazepine receptor. Pharmacol. Rev. 51, 629–650.

German, D.C., Walker, B.S., Manaye, K., Smith, W.K., Woodward, D.J., North, A.J., 1988. The human locus coeruleus: computer reconstruction of cellular distribution. J. Neurosci. 8, 1776–1788.

Ghose, S., Fujita, M., Morrison, P., Uhl, G., Murphy, D.L., Mozley, P.D., Schou, M., Halldin, C., Innis, R., 2005. Specific in vitro binding of (S,S)-[3H]MeNER to norepinephrine transporters. Synapse 56, 100–104.

Gulyás, B., Makkai, B., Kása, P., Gulya, K., Bakota, L., Várszegi, S., Beliczai, Z., Andersson, J., Csiba, L., Thiele, A., Dyrks, T., Suhara, T., Suzuki, K., Higuchi, M., Halldin, C., 2009. A comparative autoradiography study in post mortem whole hemisphere human brain slices taken from Alzheimer patients and age-matched controls using two radiolabelled DAA1106 analogues with high affinity to the peripheral benzodiazepine receptor (PBR) system. Neurochem. Int. 54, 28–36.

Haglund, M., Sjöbeck, M., Englund, E., 2006. Locus ceruleus degeneration is ubiquitous in Alzheimer's disease: possible implications for diagnosis and treatment. Neuropathology 26, 528–532.

Hall, H., Halldin, C., Farde, L., Sedvall, G., 1998. Whole hemisphere autoradiography of the postmortem human brain. Nucl. Med. Biol. 25, 715–719.

Hampel, H., Bürger, K., Teipel, S.J., Bokde, A.L., Zetterberg, H., Blennow, K., 2008. Core candidate neurochemical and imaging biomarkers of Alzheimer's disease. Alzheimers Dement. 4, 38–48.

Heneka, M.T., Galea, E., Gavriluyk, V., Dumitrescu-Ozimek, L., Daeschner, J., O'Banion, M.K., Weinberg, G., Klockgether, T., Feinstein, D.L., 2002. Noradrenergic depletion potentiates beta-amyloid-induced cortical inflammation: implications for Alzheimer's disease. J. Neurosci. 22, 2434–2442.

Heneka, M.T., Ramanathan, M., Jacobs, A.H., Dumitrescu-Ozimek, L., Bilkei-Gorzo, A., Debeir, T., Sastre, M., Galldiks, N., Zimmer, A., Hoehn, M., Heiss, W.D., Klockgether, T., Staufenbiel, M., 2006. Locus ceruleus degeneration promotes Alzheimer pathogenesis in amyloid precursor protein 23 transgenic mice. J. Neurosci. 26, 1343–1354.

Hoogendijk, W.J., Feenstra, M.G., Botterblom, M.H., Gilhuis, J., Sommer, I.E., Kamphorst, W., Eikelenboom, P., Swaab, D.F., 1999. Increased activity of surviving locus ceruleus neurons in Alzheimer's disease. Ann. Neurol. 45, 82–91.

Johansson, A., Engler, H., Blomquist, G., Scott, B., Wall, A., Aquilonius, S.M., Långström, B., Askmark, H., 2007. Evidence for astrocytosis in ALS demonstrated by [11C](L)-deprenyl-D2 PET. Neurol. Sci. 255 (1/2), 17–22.

Johnström, P., Davenport, A.P., 2005. Imaging and characterization of radioligands for positron emission tomography using quantitative phosphor imaging autoradiography. In: Davenport, A.P. (Ed.), Receptor Binding Techniques. Humana Press, New Jersey, pp. 203–216.

Kalinin, S., Gavrilyuk, V., Polak, P.E., Vasser, R., Zhao, J., Heneka, M.T., Feinstein, D.L., 2007. Noradrenaline deficiency in brain increases beta-amyloid plaque burden in an animal model of Alzheimer's disease. Neurobiol. Aging 28, 1206–1214.

Kassiou, M., Meikle, S.R., Banati, R.B., 2005. Ligands for peripheral benzodiazepine binding sites in glial cells. Brain Res. Brain Res. Rev. 48, 207–210.

Klimek, V., Stockmeier, C., Overholser, J., Meltzer, H.Y., Kalka, S., Dilley, G., Ordway, G.A., 1997. Reduced levels of norepinephrine transporters in the locus coeruleus in major depression. J. Neurosci. 17, 8451–8458.

Kelényi, G., 1967. Thioflavin S fluorescent and Congo red anisotropic staining in the histologic demonstration of amyloid. Acta Neuropathol. 7, 336–348.

Klunk, W.E., Engler, H., Nordberg, A., Wang, Y., Blomqvist, G., Holt, D.P., Bergström, M., Savitcheva, I., Huang, G.F., Estrada, S., Ausén, B., Debnath, M.L., Barletta, J., Price, J.C., Sandell, J., Lopresti, B.J., Wall, A., Koivisto, P., Antoni, G., Mathis, C.A., Långström, B., 2004. Imaging brain amyloid in Alzheimer's disease with Pittsburgh Compound-B. Ann. Neurol. 55, 306–319.

Kortvely, E., Varszegi, S., Palfi, A., Gulya, K., 2003. Intracellular targeting of calmodulin mRNAs in primary hippocampal cells. J. Histochem. Cytochem. 51, 541–544.

Kumlien, E., Bergström, M., Lilja, A., Andersson, J., Szekeres, V., Westerberg, C.E., Westerberg, G., Antoni, G., Långström, B., 1995. Positron emission tomography with [11C]deuterium-deprenyl in temporal lobe epilepsy. Epilepsia 36, 712–721.

Lyness, S.A., Zarow, C., Chui, H.C., 2003. Neuron loss in key cholinergic and aminergic nuclei in Alzheimer disease: a meta-analysis. Neurobiol. Aging 24, 1–23.

Matthews, K.L., Chen, C.P., Esiri, M.M., Keene, J., Minger, S.L., Francis, P.T., 2002. Noradrenergic changes, aggressive behavior, and cognition in patients with dementia. Biol. Psychiatry 51, 407–416.

Nordberg, A., 2007. Amyloid imaging in Alzheimer's disease. Curr. Opin. Neurol. 20, 398–402.

Nordberg, A., 2008. Amyloid imaging in Alzheimer's disease. Neuropsychologia 46, 1636–1641.

Ordway, G.A., Stockmeier, C.A., Cason, G.W., Klimek, V., 1997. Pharmacology and distribution of norepinephrine transporters in the human locus coeruleus and raphe nuclei. J. Neurosci. 17, 1710–1719.

Razifar, P., Axelsson, J., Schneider, H., Langström, B., Bengtsson, E., Bergström, M., 2006. A new application of pre-normalized principal component analysis for improvement of image quality and clinical diagnosis in human brain PET studies—clinical brain studies using [11C]-GR205171, [11C]-L-deuterium-deprenyl, [11C]-5-hydroxy-L-tryptophan, [11C]-L-DOPA and Pittsburgh vompound-B. Neuroimage 33, 588–598.

Reutens, D.C., 2000. Imaging monoamine oxidase B receptor mapping. Adv. Neurol. 83, 173–176.

Rodríguez, J.J., Olabarria, M., Chvatal, A., Verkhratsky, A., 2009. Astroglia in dementia and Alzheimer's disease. Cell Death Differ. 16, 378–385.

Sanders, J.D., Happe, H.K., Bylund, D.B., Murrin, L.C., 2005. Development of the norepinephrine transporter in the rat CNS. Neuroscience 130, 107–117.

Schou, M., Halldin, C., Sóvágó, J., Pike, V.W., Hall, H., Gulyás, B., Mozley, P.D., Dobson, D., Shchukin, E., Innis, R.B., Farde, L., 2004. PET evaluation of novel radiofluorinated reboxetine analogs as norepinephrine transporter probes in the monkey brain. Synapse 53, 57–67.

Schou, M., Halldin, C., Pike, V.W., Mozley, P.D., Dobson, D., Innis, R.B., Farde, L., Hall, H., 2005. Post-mortem human brain autoradiography of the norepinephrine transporter using (S,S)-[18F]FMeNER-D2. Eur. Neuropsychopharmacol. 15, 517–520.

Schroeter, S., Apparsundaram, S., Wiley, R.G., Miner, L.H., Sesack, S.R., Blakely, R.D., 2000. Immunolocalization of the cocaine- and antidepressant-sensitive l-norepinephrine transporter. J. Comp. Neurol. 420, 211–232.

Schwab, C., McGeer, P.L., 2008. Inflammatory aspects of Alzheimer disease and other neurodegenerative disorders. J. Alzheimers Dis. 13, 359–369.

Seneca, N., Gulyás, B., Varrone, A., Schou, M., Airaksinen, A., Tauscher, J., Vandenhende, F., Kielbasa, W., Farde, L., Innis, R.B., Halldin, C., 2006. Atomoxetine occupies the norepinephrine transporter in a dose-dependent fashion: a PET study in nonhuman primate brain using (S,S)-[18F]FMeNER-D2. Psychopharmacology (Berl) 188, 119–127.

Smith, H.R., Beveridge, T.J., Porrino, L.J., 2006. Distribution of norepinephrine transporters in the non-human primate brain. Neuroscience 138, 703–714.

Svedberg, M.M., Hall, H., Hellström-Lindahl, E., Estrada, S., Guan, Z., Nordberg, A., Långström, B., 2009. [(11)C]PIB-amyloid binding and levels of Abeta40 and Abeta42 in postmortem brain tissue from Alzheimer patients. Neurochem. Int. 54, 347–357.

Szot, P., Leverenz, J.B., Peskind, E.R., Kiyasu, E., Rohde, K., Miller, M.A., Raskind, M.A., 2000. Tyrosine hydroxylase and norepinephrine transporter mRNA expression in the locus coeruleus in Alzheimer's disease. Brain Res. Mol. Brain Res. 84, 135–140.

Szot, P., White, S.S., Greenup, J.L., Leverenz, J.B., Peskind, E.R., Raskind, M.A., 2006. Compensatory changes in the noradrenergic nervous system in the locus ceruleus and hippocampus of postmortem subjects with Alzheimer's disease and dementia with Lewy bodies. J. Neurosci. 26, 467–478.

Takano, A., Gulyás, B., Varrone, A., Karlsson, P., Schou, M., Airaksinen, A.J., Vandenhende, F., Tauscher, J., Halldin, C., 2008a. Imaging the norepinephrine transporter with positron emission tomography: initial human studies with (S,S)-[(18)F]FMeNER-D(2). Eur. J. Nucl. Med. Mol. Imaging 35, 153–157.

Takano, A., Halldin, C., Varrone, A., Karlsson, P., Sjöholm, N., Stubbs, J.B., Schou, M., Airaksinen, A.J., Tauscher, J., Gulyás, B., 2008b. Biodistribution and radiation dosimetry of the norepinephrine transporter radioligand (S,S)-[(18)F]FMeNER-D(2) a human whole-body PET study. Eur. J. Nucl. Med. Mol. Imaging 35, 630–636.

Takano, A., Varrone, A., Gulyás, B., Karlsson, P., Tauscher, J., Halldin, C., 2008c. Mapping of the norepinephrine transporter in the human brain using PET with (S,S)-[18F]FMeNER-D2. Neuroimage 42, 474–482.

Takano, A., Gulyás, B., Varrone, A., Halldin, C., 2009a. Comparative evaluations of norepinephrine transporter radioligands with reference tissue models in rhesus monkeys: (S,S)-[18F]FMeNER-D2 and (S,S)-[11C]MeNER. Eur. J. Nucl. Med. Mol. Imaging 36, 1885–1891.

Takano, A., Gulyás, B., Varrone, A., Maguire, R.P., Halldin, C., 2009b. Saturated norepinephrine transporter occupancy by atomoxetine relevant to clinical doses: a rhesus monkey study with (S,S)-[(18)F]FMeNER-D (2). Eur. J. Nucl. Med. Mol. Imaging 36, 1308–1314.

Tejani-Butt, S.M., Yang, J., Zaffar, H., 1993. Norepinephrine transporter sites are decreased in the locus coeruleus in Alzheimer's disease. Brain Res. 631, 147–150.

Tellioglu, T., Robertson, D., 2001. Genetic or acquired deficits in the norepinephrine transporter: current understanding of clinical implications. Expert Rev. Mol. Med. 19, 1–10.

Thal, D.R., Braak, H., 2005. Post-mortem diagnosis of Alzheimer's disease. Pathologe 26, 201–213.

Tuohy, E., Leahy, C., Dockery, P., Fraher, J., Fitzgerald, E., Galvin, R., Dansie, P., 2004. An anatomical and MRI study of the human thalamus. J. Anat. 204, 527–528.

Varnäs, K., 2005. Distribution of Serotonin Receptors and Transporters in the Human brain: Implications for Psychosis. PhD Thesis. Karolinska Institute.

Varnäs, K., Halldin, C., Hall, H., 2004. Autoradiographic distribution of serotonin transporters and receptor subtypes in human brain. Hum. Brain Mapp. 22, 246–260.

Venneti, S., Lopresti, B.J., Wiley, C.A., 2006. The peripheral benzodiazepine receptor (translocator protein 18 kDa) in microglia: from pathology to imaging. Prog. Neurobiol. 80, 308–322.

Vizi, E.S., 2000. Role of high-affinity receptors and membrane transporters in nonsynaptic communication and drug action in the central nervous system. Pharmacol. Rev. 52, 63–89.

Wilson, A.A., Johnson, D.P., Mozley, D., Hussey, D., Ginovart, N., Nobrega, J., Garcia, A., Meyer, J., Houle, S., 2003. Synthesis and in vivo evaluation of novel radiotracers for the in vivo imaging of the norepinephrine transporter. Nucl. Med. Biol. 30, 85–92.

Zarow, C., Lyness, S.A., Mortimer, J.A., Chui, H.C., 2003. Neuronal loss is greater in the locus coeruleus than nucleus basalis and substantia nigra in Alzheimer and Parkinson diseases. Arch. Neurol. 60, 337–341.